The First Terrestrial Electron Beam Observed by The Atmosphere-Space Interactions Monitor

D. Sarria[1], P. Kochkin[1], N. Østgaard[1], N. Lehtinen[1], A. Mezentsev[1], M. Marisaldi[1], B.E. Carlson[1,2], C. Maiorana[1], K. Albrechtsen[1], T. Neubert[3], V. Reglero[4], K. Ullaland[1], S.Yang[1], G. Genov[1], B. H. Qureshi[1], C. Budtz-Jørgensen[3], I. Kuvvetli[3], F. Christiansen[3], O. Chanrion[3], M. Heumesser[3], K. Dimitriadou [3], J. Navarro-González[4], P. Connel[4], C. Eyles[4]

[1]Birkeland Centre for Space Science, University of Bergen, Bergen, Norway
[2]Carthage College, Kenosha, Wisconsin, United States
[3]National Space Institute, Technical University of Denmark, Lyngby, Denmark
[4]University of Valencia, Valencia, Spain

Key Points:

- Flying over an area with no nearby lightning activity, the ASIM-MXGS instrument detected a four ms long event with a soft spectrum.
- Observations coupled with simulations suggest that more than 90% of the counts come from a TEB, and the rest from the associated TGF.
- A source TGF with a broad angular distribution and 10^{17} to 10^{19} photons can explain the observation.

Corresponding author: D. Sarria, david.sarria@uib.no

Abstract

We report the first Terrestrial Electron Beam (TEB) detected by the Atmosphere-Space Interactions Monitor (ASIM). It happened on September 16th, 2018. The ASIM Modular X and Gamma-ray Sensor (MXGS) recorded a two millisecond long event, with a softer spectrum than typically recorded for Terrestrial Gamma-ray Flashes (TGF). The lightning discharge associated to this event was found in the World-Wide Lightning Location Network (WWLLN) data, close to the northern footpoint of the magnetic field line passing by the International Space Station (ISS). Imaging from a GOES-R geostationary satellite shows that the source TGF was produced close to an overshooting top of a thunderstorm. Monte-Carlo simulations were performed to reproduce the observed lightcurve and energy spectrum. The event can be explained by the secondary electrons and positrons produced by the TGF (i.e. the TEB), even if about 5% to 10% of the detected counts may be due to direct TGF photons. A source TGF with a Gaussian angular distribution with standard deviation between 21^o and 29^o was found to reproduce the measurement. Assuming an isotropic beaming within a cone, compatible half angles are between 29^o and 43^o, in agreement with previous studies. The number of required photons for the source TGF could be estimated for various assumption of the source (altitude of production, angular distribution), and is estimated between 10^{17} and 10^{18} photons, i.e. compatible with the current consensus.

Plain Language Summary

Terrestrial Gamma-Ray Flashes (TGFs) are the highest energy natural particle acceleration phenomena occurring on Earth. They are burst of energetic photons associated with thunderstorms, and have a poorly understood production mechanism. When interacting with the atmosphere, TGFs produce secondary electrons and positrons of high energy. A fraction of them can reach Space, and forms a beam under the effect of Earth's magnetic field, so called Terrestrial Electron Beam (TEB). They can be detected over geographical location with no lightning activity. In the past, TEBs have been detected by the Fermi space telescope and the Compton Gamma-ray Observatory. In this article, we report the first detection of a TEB by the Atmosphere-Space Interactions Monitor (ASIM), docked on the International Space Station since April 2018. During this event, no lightning activity was detected below the instrument. The TEB's source lightning was actually found to be located 650 away from detector, very close to an overshoot-

ing top of a thundercloud. The comparison of the observation with simulated data made it possible to constrain the geometry of the parent TGF. Our results point towards a relatively wide angular distribution and an intensity of 10^{17} to 10^{19} photons, in agreement with previous studies.

1 Introduction

Terrestrial Gamma-ray Flashes (TGFs) are short ($<$ 2 ms) bursts of high energy ($<$ 30-40 MeV) photons, produced during thunderstorms, between 10 and 15 km altitude, for events detectable from space. A review of the science of TGFs is presented by Dwyer et al. (2012). TGFs were first detected using the BATSE experiment on-board the NASA's CGRO spacecraft. Later, TGFs were recorded from space by RHESSI (Smith et al., 2005), AGILE (MCAL instrument) (Marisaldi et al., 2014), the Fermi space telescope (GBM instrument) (Briggs et al., 2010; Roberts et al., 2018), BeppoSAX (Ursi et al., 2017) and the Atmosphere-Space Interactions Monitor (ASIM) (Neubert, Østgaard, Reglero, Blanc, et al., 2019). This last is the only one specifically designed to detect TGFs from space, using the Modular X- and Gamma-ray Sensor (MXGS) (Østgaard et al., 2019). ASIM was successfully launched and docked to the International Space Station in April 2018, and started science operations in June 2018. The first results from ASIM are presented in (Neubert, Østgaard, Reglero, Chanrion, et al., 2019; Østgaard et al., 2019), in addition to this article.

TGFs deposit a large amount of energy in the atmosphere, as a large fraction (typically $>$ 97%) of the initial bremsstrahlung photons is absorbed before reaching space. By colliding with the atmosphere, the photons produce a large quantity of electrons (through Compton scattering and pair production) and positrons (pair production), but only a small fraction is able to escape the atmosphere. Most of the escaping electrons are produced above $\approx$40 km altitude (Sarria et al., 2015). Once they have escaped, the electrons and positrons are then bounded to Earth's magnetic field lines and can travel large distances inside the magnetosphere (Dwyer et al., 2008; Briggs et al., 2011). This phenomenon is called a Terrestrial Electron Beam (TEB). The TGF responsible for the TEB will be referred as the "source TGF" in the rest of this article. TEBs were first reported from measurements of the BATSE/CGRO spacecraft (Dwyer et al., 2008). Later, they were detected by the Fermi space telescope (Briggs et al., 2011), and one event was found in the BeppoSAX satellite data archive (Ursi et al., 2017). The duration of TEBs is sev-

eral times larger that TGFs. This is because the electrons/positrons have a wide range of pitch angles (with respect to the local magnetic field direction) when they are produced and/or escape the atmosphere, which leads to a temporal dispersion after propagating several thousand of kilometers along Earth's magnetic field lines. This phenomenon is illustrated in figure 1. For more information about the pitch angle distribution of TEB's electrons, see Sarria et al. (2016). A TEB typically contains 8% to 15% of positrons. All TGFs directed to space produce a TEB, but they are more difficult to detect than TGF. This is because a TGF can be detected by satellites located within a radius of about 800 km around its source, whereas TEBs extend only over a few tens of kilometers around the two point where the magnetic field line reaches the altitude of the satellite (in some cases, the magnetic field line does not even reach the altitude of the satellite). For example, the first Fermi-GBM TGF catalog presents only 30 TEB candidates among the total of 4135 listed TGF events (Roberts et al., 2018).

In this article we report the first TEB event detected by ASIM, using the MXGS instrument. Although the MXGS primary objective is to detect TGFs, a long trigger window (25 milliseconds) was implemented to detect longer events like TEBs. In section 2, we present the ASIM-MXGS instrument and discuss its ability to detect TEBs. In section 3, we present the event detected on September 16th, 2018. In section 4, we use Monte-Carlo simulation in order to reproduce the event and to constrain its beaming and its source content. We conclude in section 5.

2 Instruments and data

The Atmosphere-Space Interactions Monitor (ASIM) (Neubert, Østgaard, Reglero, Blanc, et al., 2019) consists of two main instruments : MXGS (Modular X- and Gamma-ray detector) for hard radiation observations and MMIA (Modular Multi-spectral Imaging Array) for optical observations (Chanrion et al., 2019). The MXGS instrument consists of a Low Energy Detector (LED) and a High Energy Detector (HED). Østgaard et al. (2019) described the instrument in details. The HED is based on twelve Bismuth Germanium Oxide (BGO) scintillator crystal bars of 15 x 5 x 3.2 cm^3 interfaced to Photomultiplier tubes, and is sensitive to energies of $\sim$200 keV to $\sim$40 MeV. It has a total geometrical area of 900 cm^2. The LED consists of an array of Cadmium-Zink-Telluride (CZT) detector crystals with a total of 16384 pixels, and geometrical area of 1024 cm^2. It operates in the energy range of $\sim$20 keV to $\sim$400 keV. The LED only operates during nigh-

time, and the event reported in this article happened during daytime. MXGS uses 4 trigger time windows: 300 μs, 1 ms, 3 ms and 25 ms, this last being specifically implemented to target TEBs. For both detectors, if the recorded number of count exceeds a given threshold within one of these time windows, the MXGS instrument triggers, and saves high resolution data of every single recorded count inside a time frame of approximately ± 1 second around the trigger time.

ASIM is mounted to the Columbus module on the International Space Station (ISS) since April 2018. The ISS has been designed to always show the same side to the Earth, meaning that MXGS is always pointing towards the nadir. Let θ be the angle, measured from the ISS, between the nadir and the location of a TGF. All TGF events are expected to come with $\theta < 70^o$. TEB's electrons and positrons are bounded to Earth's magnetic field lines and perform helical motion around it and therefore can hit the space station from any angle of incidence.

In order to simulate the response of MXGS to TGF and TEB, we developed a complete mass model of the instrument (Østgaard et al., 2019), based on the Geant4 toolkit (Agostinelli et al., 2003; Allison et al., 2006, 2016). It includes all relevant elements around the instrument, in particular the HED, LED, coded mask, shielding and electronics, MMIA, mounting platform, the other mounted instruments, and the Columbus module. By Monte-Carlo simulations we estimated that the effective area of the HED for a typical TEB is about 150 cm^2, which is about 25% of the one for a typical TGF. In this case the effective area is calculated as the geometrical area ($\approx$ 900 cm^2 for HED and $\approx$ 1024 cm^2 for LED) multiplied by the probability of an incident TEB electron to deposit more than 400 keV into at least one BGO crystal. This energy deposition can be direct (electrons hitting the crystal) or indirect. In the indirect case, electrons emit bremsstrahlung photons by interaction with the surrounding material, that hit at least one BGO crystal. For HED, the indirect process is mostly involved during TEB events, because of the shielding around the crystals that will absorb most of the electrons. The effective area is function of the energy of the electron, and the value given previously is an average over a typical TEB spectrum. We also estimated that the effective area of the LED detector for TEB detection is about 280 cm^2. It is significantly larger than for HED because direct electron hits are much more likely. It implies that, during a TEB event, the LED could detect twice more particles than the HED. This prediction should be testable with future events, since the LED was not operating for the event reported here.

3 Observation

ASIM-MXGS recorded an unusually long event on September 16th, 2018, at 13:14:44.733601 (UTC). The event was strong enough to have been triggered by the 3 ms window. The recorded lightcurve is presented in figure 2. The event consists of pulse of more than 2 ms duration, and does not present any mirror pulse. The small increase around 13 ms is just due to background fluctuations. Figure 3.a. shows the geometry of the event on a map. Table 1 gives a summary of the coordinates and times of the interesting points. The event occurred when the ISS was located at a latitude $\lambda = 6.28^{\circ}$, a longitude $\phi = -95.71^{\circ}$ and an altitude of 402.5 kilometers (geodetic coordinates). The data from World Wide Lightning Location Network (WWLLN) was also used for this analysis. It provides lightning timing and location by the use of a network of VLF sensors positioned on the ground around the globe. According to WWLLN, there was no lightning activity below the ISS within a reasonable time window (few minutes) and distance (< 600 km). We could estimate the position of the magnetic field line footpoint at 45 km altitude (approximately the altitude where most of the electrons that have a chance to escape the atmosphere are produced) in the northern hemisphere to be at coordinates $\lambda = 11.08^{\circ}$, $\phi = -95.40^{\circ}$ (geodetic). This position was obtained from the model presented in Emmert et al. (2010), based on IGRF-12 (Thébault et al., 2015). These geographic coordinates were also confirmed by the two other codes, implementing the IGRF-12 model and a Runge-Kutta stepper to propagate the electrons/positrons along Earth's magnetic field (MC-PEPTITA and Geant4-based) that will be presented in section 4. Six WWLLN events were found around this location, within a time frame of less than 140 ms. Three of them are within 6 ms, well within the MXGS absolute timing uncertainty of about 20 ms. Since these three events happened within 0.1 ms, they belong to the same flash. The coordinates of these three WWLLN events are given in Table 1 as events 4-6. They are respectively 11.72 km, 13.79 km and 12.69 km away from the northern magnetic field line footpoint at 45 km altitude, knowing that the WWLLN has a generic positioning uncertainty of ± 15 km. The probability of having a WWLLN event in such a narrow time window and position by random chance is extremely low. Therefore these three points are likely close to the location of a lightning flash associated with a TGF that generated a TEB that was recorded by MXGS. In addition, simulated data, presented in section 4, also indicate that the duration of the observation is compatible with a TEB event, and that the time between the TGF production and the first electron reaching the detector is about

2.3 ms, which is close to travel time at the speed of light along the magnetic field line. Simulated data also indicate that 95% of the electron/positron beam is contained in an ellipse of semi-major axis of ≈ 88 km and semi-minor axis of ≈ 54 km.

As it has been observed previously (see e.g. Briggs et al. (2011); Ursi et al. (2017)), a TEB could, in principle, come from a source TGF located at the magnetic footpoint of the opposite hemisphere. For this event, it is located at $\lambda = -29.86$ °, $\phi = -101.02$ °(geodetic). However, we could not find any WWLLN match near this point within a reasonable time frame. Furthermore, according to simulations, the observed TEB duration in this configuration should be about 20 ms, which is substantially longer than our observation (as discussed in next section, and see also figure 2).

Figure 3.a. shows an image of the thunderstorm system located around the north magnetic field line footpoint, obtained by the geostationary satellite GOES-16 and has 0.5 km spatial resolution (Advanced Baseline Imager band 2, visible red, centered at 0.64 μm). The image was taken around 13:15:30 (UTC), i.e. about 45 seconds after the ASIM trigger. The positions of the three closeby WWLLN events are presented, and all are within 6 ms of the ASIM trigger time. They also appear close to an overshooting top of the thunderstorm system. Overshooting tops correspond to a region with high convective activity, with a high lightning activity in the vicinity, therefore it is not surprising if this region of the cloud generated a TGF..

4 Monte-Carlo simulations of the event

Numerical Monte-Carlo simulations were performed to reproduce the recorded lightcurves and energy spectrum of the event. As this event shows a relatively low flux (i.e. particle count rate), it was possible to get a reliable calibration of the instrument. Two models were used to propagate the TGF and secondary particles from the source of the TGF to ASIM: the MC-PEPTITA model (Sarria et al., 2015) and a new model based on the Geant4 toolkit (Agostinelli et al., 2003; Allison et al., 2006, 2016). The Geant4-based code is made publicly available (see acknowledgments) and presented into more details in appendix A. Both models are able to propagate photons, electrons and positrons in Earth's environment, including the atmosphere and the Earth's magnetic field. They include the relevant processes for photons (Compton scattering, photo-electric absorption, pair production, Rayleigh scattering) and electron/positron transport (elastic/inelastic

scattering, bremsstrahlung, annihilation). For simplicity, we only show results from the Geant4-based model, as both models showed very consistent results in all the simulations we performed.

The simulations start from a time instantaneous photon source, with a bremsstrahlung energy spectrum $\propto 1/\epsilon \times \exp(-\epsilon/7.3\,\mathrm{MeV})$. The TGF is located at 15 km altitude (later in this section an altitude range between 10 and 16 km is tested), pointing towards zenith, with an opening angle that can be isotropic or Gaussian. The isotropic angular distribution is parameterized by the opening half-angle θ, and the Gaussian by the standard deviation σ_θ. The time reference is set to the source TGF production time, assumed to be located at the coordinates of the northern or southern magnetic footpoints. Figure 1 illustrates the geometry of the simulation, and explains why TEBs are temporally more dispersed than TGFs, and shows the pitch angle distribution as a function of arrival time that was obtained for this event. If the TGF is located at the north footpoint ($\lambda = 11.01^o$, $\phi = -95.40^o$, geodetic coordinates), it takes about 2.28 ms for a direct photon (straight line) to travel from their source to the ISS (located about 650 km away), and the fastest electron/positron arrives about 48 μs later. The pointing angle between the ISS and the TGF source is about 58.4° with respect to nadir.

Figure 2.a. presents a comparison between the observed lightcurve, and the simulations. For all the simulations, except the yellow histogram, we assumed that the TGF was produced close to the northern footpoint of the magnetic field line passing by the ISS. The simulated TEB lightcurve (electrons/positrons) is compatible with the measurement. The simulations also confirm that there is no mirror pulse detectable above the background level for this geographical configuration (it would be located between 60 and 75 ms). The yellow histogram presents the lightcurve that would be observed if the TGF had been produced in the southern footpoint of the magnetic field line, and shows a signal about 4 times longer that the observation ($\sim$ 20 ms compared to $\sim$ 5 ms). Figure 2.b. shows the same lightcurves, zoomed-in between 2.1 and 3.1 ms. According to the simulation, the signal due to the photons from the TGF (produced $\approx$ 650 km away from the ISS) should be above the background level, and have a duration of about 240 microseconds. The pulse due to TGF photons is about 20 times shorter than the one due to the TEB, that lasts about 5 milliseconds. It indicates that some of the direct photons from the TGF may also have been detected. This fraction will depend on the location of the ISS with respect to the center of the electron/positron beam and, more impor-

tantly, on the angular distribution of the TGF. Figure 4.a. and b. presents the same comparison as before, but assuming several angular distributions for the source TGF. Compared to figure 2, the relative effective areas of MXGS to detect photons (~ 650 cm^2) and electrons/positrons (~ 150 cm^2) were taken into account. A change in the TGF angular distribution parameter mostly affects the counts inside the second bin of the histogram (located between 2.1 and 2.3 ms), containing mainly photons. For the isotropic (within a cone) angular distribution, the observed lightcurve is compatible with the simulations if a half-angle of θ between $\approx 29^o$ and $\approx 43^o$ is assumed. For the Gaussian angular distribution, it is for a σ_θ between $\approx 21^o$ and $\approx 29^o$. This range is in agreement with previous studies (Dwyer & Smith, 2005; Østgaard et al., 2008; Hazelton et al., 2009; Carlson et al., 2011; Mailyan et al., 2016). This scenario implies that about 8 to 15 of the recorded counts by ASIM-MXGS are actually direct TGF photons, that arrive mostly at the beginning of the recorded lightcurve. This is about 5 to 10 % of the total number of counts ($\sim$160). Our analysis assumes that the TGF source is instantaneous, and should not change significantly if the TGF is less than 20 μs at source, as the simulated photon pulse has a total duration of about 2 ms (see Figure 2.b). Assuming a larger TGF duration at source would increase the estimated values of θ and σ_θ.

Figure 5 presents the recorded background-subtracted energy spectrum comparison between the measurement and the simulation. The spectrum is actually softer than what is recorded during usual TGF events. The simulations use the ASIM Geant4 mass model presented by Østgaard et al. (2019). Two scenarios were considered, one assuming the incoming particles are photons from the TGF, and the other assuming the incoming particles are the secondary electron/positrons. The TGF and TEB spectra used as input for the MXGS mass model were calculated using a Geant4-based model of TGF propagation in the atmosphere with the assumptions presented preivously. The particles used as input for the ASIM mass model were gathered at 400 km altitude, around the position of the ISS ($\pm$80 km). The quality of the simulated data compared to the observation can be quantified using the reduced chi squared (χ^2_{red}). The χ^2_{red} values obtained for the simulated response to a TGF and to a TEB are 7.2 and 1.13, respectively. Due to the chosen energy binning, there are 7 degrees of freedom, and using a usual 95% probability threshold, it gives a critical value $\chi^2_{red,c}$ equal to 2.01. It means that the TEB model, with $\chi^2_{red} < \chi^2_{red,c}$, is compatible with the measurement, whereas the TGF model, with $\chi^2_{red} > \chi^2_{red,c}$, is not. In addition to the results concerning the lightcurve (previ-

ous paragraph), and the geographical and time lightning matches (section 3), we think that it is enough evidence to consider that this event is mostly a TEB, with a small fraction (5% to 10%) of photons coming directly from the TGF.

Finally, we can estimate the required photons number N_γ of the source TGF in order to obtain the ≈160 counts that were observed by HED. The exact value of N_γ depends on assumptions of the source TGF, mainly the altitude of production and the angular distributions. We performed a series of simulation using the Geant4-based model, with a TGF altitude of production tested between 10 and 16 km, assuming an isotropic distribution of photons within a cone (with parameter the half-angle of the cone, θ, tested from 10° to 50°), or a Gaussian distribution (with parameter the standard deviation σ_θ, tested from 10° to 40°). The results are presented in figure 6. Taking into account the constraints on the angular distributions discussed before, a value of N_γ of about 10^{17} (high altitude) up to about 10^{19} photons (low altitude) is required to reproduce the measurement. This range is in agreement with values given by previous studies (Dwyer & Smith, 2005; Dwyer et al., 2012; Cummer et al., 2014; Gjesteland et al., 2015).

5 Conclusions and future work

We reported the first TEB detected by the MXGS-HED instrument on-board the Atmosphere-Space Interactions Monitor (ASIM). It appeared as an unusually long event ($>$ 2 ms) with a spectrum softer than what is usually seen from TGF events. Tracing of the geomagnetic field line from the ISS permitted to estimate a likely geographical position of the TGF that produced the TEB, where three WWLLN matches within compatible time ($<$6 ms) and distance ($<$15 km) intervals were found. From geostationary imaging, obtained just about 45 seconds after the event, it appears that the TGF was produced in the vicinity of an overshooting top of a thunderstorm.

Using Monte-Carlo simulations to reproduce the observed lightcurve and energy spectrum, we show that the event is indeed mostly explained by a TEB, even if 5% to 10% of the detected flux may be direct TGF photons. A source TGF with a broad angular distribution can explain the observation ($\theta \approx 30^o - 45^o$ for a uniform distribution, or $\sigma_\theta \approx 20^o - 30^o$ for a Gaussian distribution). The intensity of the source TGF could be estimated for various assumptions of the source (altitude of production, angu-

	Time (UTC)	λ(°)	ϕ(°)		
Magnetic footpoint (North, h=45 km)	N.A.	11.08	-95.40		
ISS	13:14:44.733601	6.28	-95.71	Δt, ms (w.r. trigger time)	Δr, km (w.r. magn. footpoint)
WWLLN event #1	13:14:44.601058	6.37	-89.375	132.543	895.77
WWLLN event #2	13:14:44.601059	6.43	-89.26	132.541	902.05
WWLLN event #3	13:14:44.700633	6.41	-89.30	32.968	899.78
WWLLN event #4	13:14:44.738832	11.08	-95.50	-5.232	11.72
WWLLN event #5	13:14:44.738894	11.03	-95.29	-5.293	13.79
WWLLN event #6	13:14:44.738925	11.08	-95.29	-5.324	12.69

Table 1. Summary table of the time and coordinates of the interesting elements for the ASIM event that happened on 2018/09/16. WWLLN events number 4, 5 and 6 are in a very narrow time (with respect to the event trigger time) and distance windows (with respect to the northern magnetic field line footpoint) and can be considered as good matches for the lightning discharge that produced the TGF. Due to their very narrow time differences (< 0.1 ms), these three matches probably belong to the same discharge.

lar distribution), and is between 10^{17} and 10^{19} photons. This range is in agreement with commonly accepted values.

Here, we have discussed a TEB event detected during the daytime by the HED instrument alone. Future observations during nighttime have the added promise of simultaneous detection by the LED and MMIA instruments. It will allow measurements of the low-energy part of the spectrum (∼20 keV to ∼400 keV), and hypothetical UV and optical emissions associated with such events.

Planned for a launch in 2020, the TARANIS micro-satellite (Lefeuvre et al., 2009), should also detect TEB events. It is primarily designed to detect both TGFs and TEBs, with help of the XGRE and IDEE instruments (Sarria et al., 2017), and will have, in addition, the capability of detecting hypothetical radio emissions from TEBs.

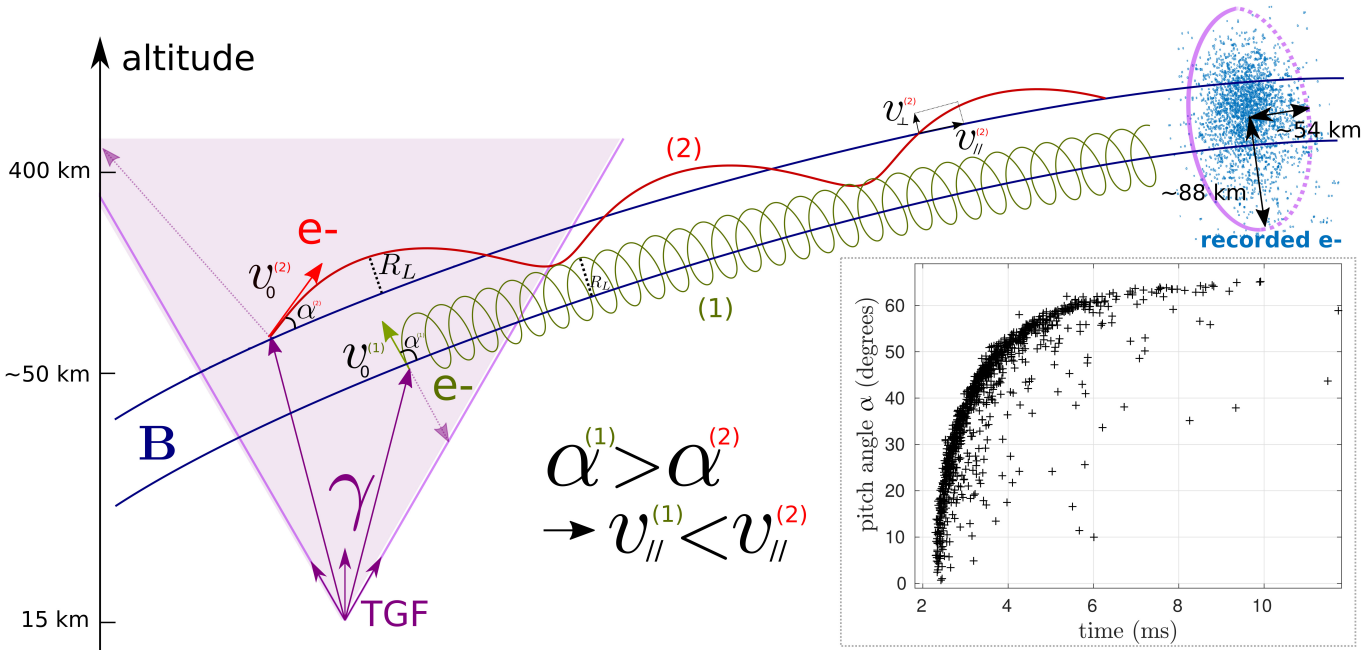

Figure 1. This sketch illustrates why the time distribution for a TEB event is mainly due to the pitch angle α with respect to Earth's magnetic field. Most of the electrons/positrons are relativistic and hence have a speed close to the speed of light. However, they have to follow helical trajectories around the field lines, and the electrons/positrons with larger α will undergo more rotations around the field lines, and with a larger Larmor radius (R_L) at the same electron energy, before reaching the satellite. They have actually a smaller velocity along the field line ($v_{//}$). More energetic electrons will have a larger R_L (as it is proportional to the Lorentz's γ factor). The insert shows the pitch angle as function of arrival time (according to the simulations described in section 4). At the satellite level, most of the electrons will arrive inside an ellipse of 54 km semi-minor axis and 88 km semi-major axis.

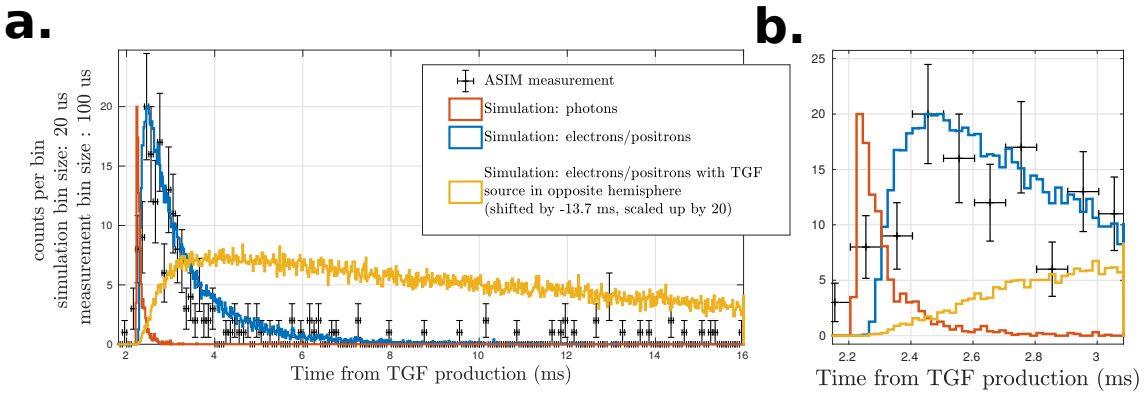

Figure 2. **a.** Comparison between simulated and measured lightcurves for the TEB event. Time 0 is when the source TGF is produced. The signal of the photons (TGF part) and electron/positron beams (TEB part) are shown. The relative scale between the photons and the electron/positron components was adjusted for visibility.

The observed lightcurve matches the electron/positron component (TEB) of September 16th, 2018. The yellow histogram presents the TEB lightcurve that would be observed if the associated TGF was produced in the southern footpoint of the magnetic field line, and shows a signal about 5 times longer that the observation. It was scaled in amplitude by a factor of 20 and shifted in time by -13.7 ms, to be able to display it inside the same time scale. **b.** Zoomed in between 2.1 and 3.1 ms. The simulations indicate that photons from the TGF could also have been observed, and they should be mostly within the first 0.2 ms of the event. According to this simulation, most of the recorded counts below about 2.3 ms are due to photons.

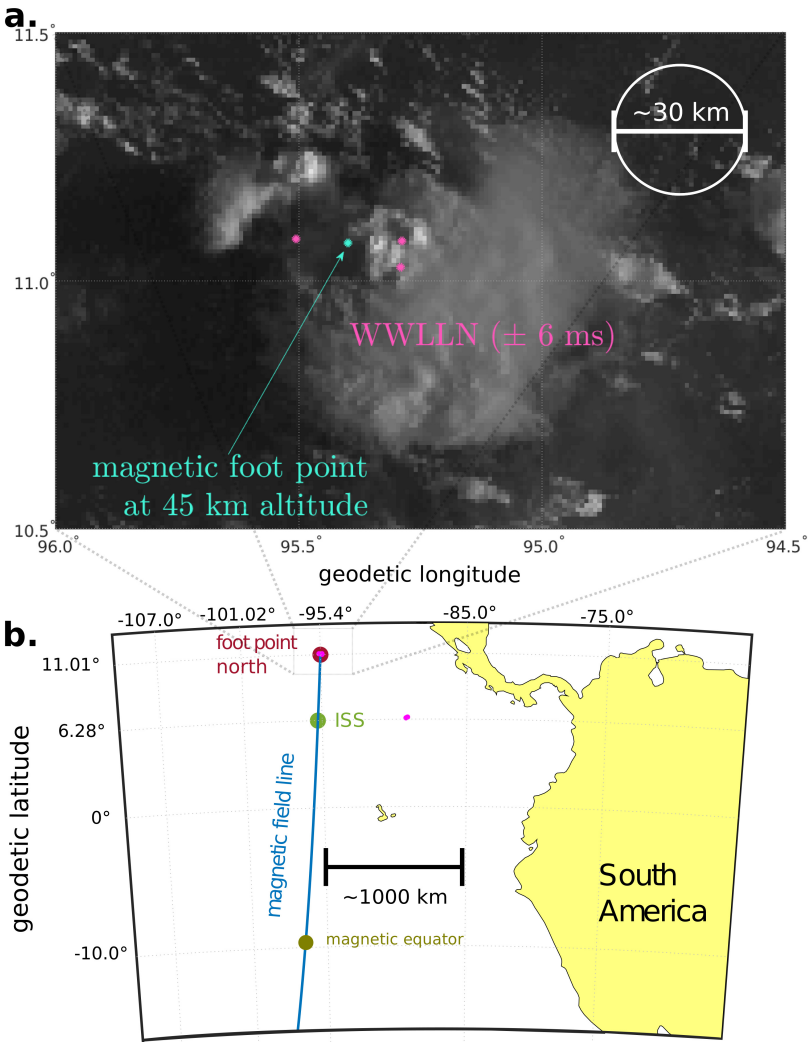

Figure 3. **a.** Image from geostationary satellite GOES-16 on September 16th, 2018, around 13:15:30 UTC (about 45 seconds after ASIM trigger time), zoomed around the north footpoint region. The image comes from the Advanced Baseline Imager instrument, optical band 2, centered at 0.64 μm, with 0.5 km resolution. The three closest positions obtained from WWLLN are presented, that may correspond to a single discharge. They are within 6 ms of the ASIM trigger time (MXGS absolute timing uncertainty is about 20 ms) and within 15 km of the northern magnetic footpoint (WWLLN generic positioning uncertainty is ±15 km). The four points are located close to an overshooting top of the thunderstorm system. **b.** The map shows the positions of interesting points of the event. The ISS (green dot) is located at a latitude $\lambda = 6.28°$ and a longitude $\phi = -95.71°$ (geodetic). The two red dots are the magnetic footpoints of the magnetic field line passing though the ISS (coordinates $\lambda = 10.98°$, $\phi = -95.39°$ and $\lambda = -29.64°$, $\phi = -101.09°$, geodetic). The corresponding magnetic latitude is 21.05° (modified apex). The small magenta dots are the position of the lightning discharges obtained from WWLLN sferic detections, within a time frame of 140 milliseconds around the ASIM trigger time.

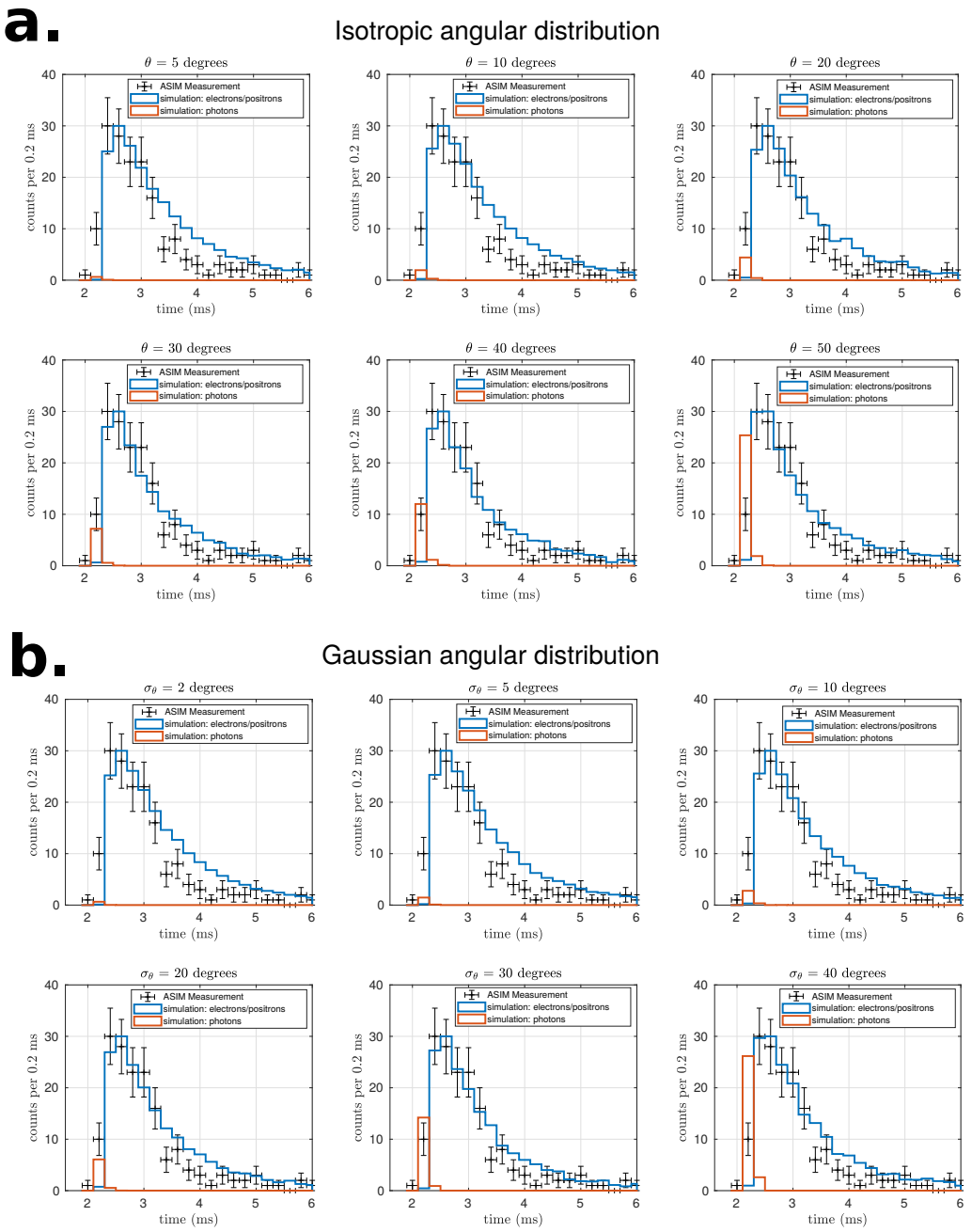

Figure 4. Comparison of the simulated and measured lightcurves . Error bars indicate a 1-σ interval. Assuming various opening angle of the source TGF (that produced the TEB). Compared to figure 2, the relative fluxes between electrons/positrons and photons take now into account the efficiency of the detector for the different particles. **a.** Isotropic angular distribution inside a cone, with half angle θ. **b.** Gaussian (normal) angular distribution with standard deviation σ_θ. The observed lightcurve is compatible with the simulations if we assume an half-angle of θ between 29.2 and 42.7 degrees for the isotropic case. For the Gaussian case, it is for a σ_θ between 20.9 and 28.7 degrees. Here, the compatibility criteria is chosen as if the second red bin count (photons arriving between 2.1 and 2.3 ms) is inside the 1-σ error interval of the ASIM measurement.

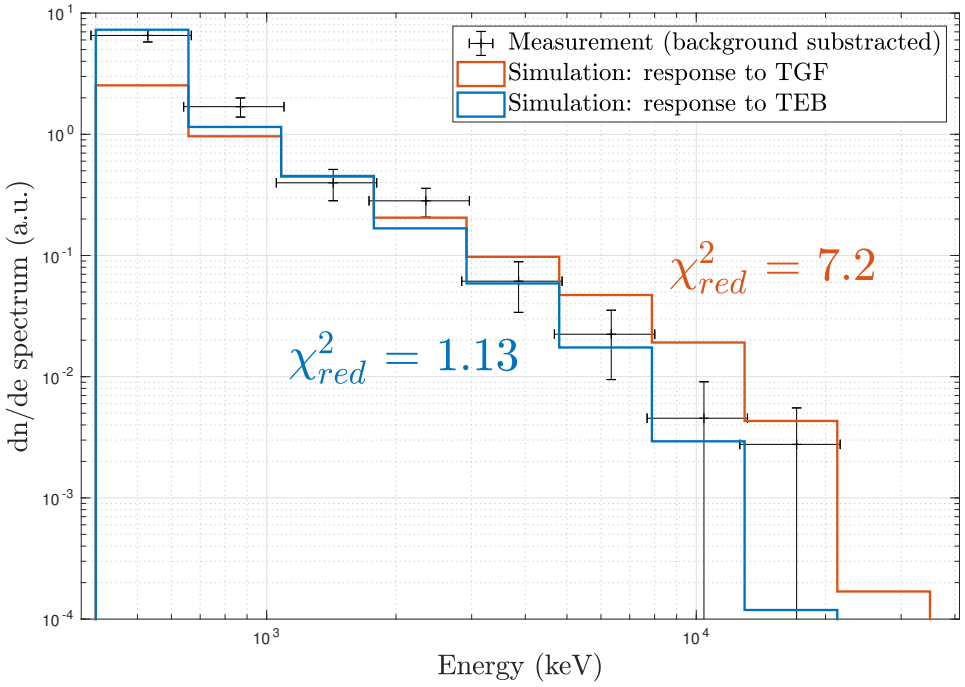

Figure 5. Energy spectrum comparison between the ASIM-MXGS measurement and simulations. Two simulation scenario were considered: incoming particles are from TGF or TEB. The two simulated spectra are scaled to minimize the values of χ^2_{red}, which are indicated. They give an indication of the agreement between simulation and measurement (a lower value indicates a better agreement). The response to TEB fits better to the measurement.

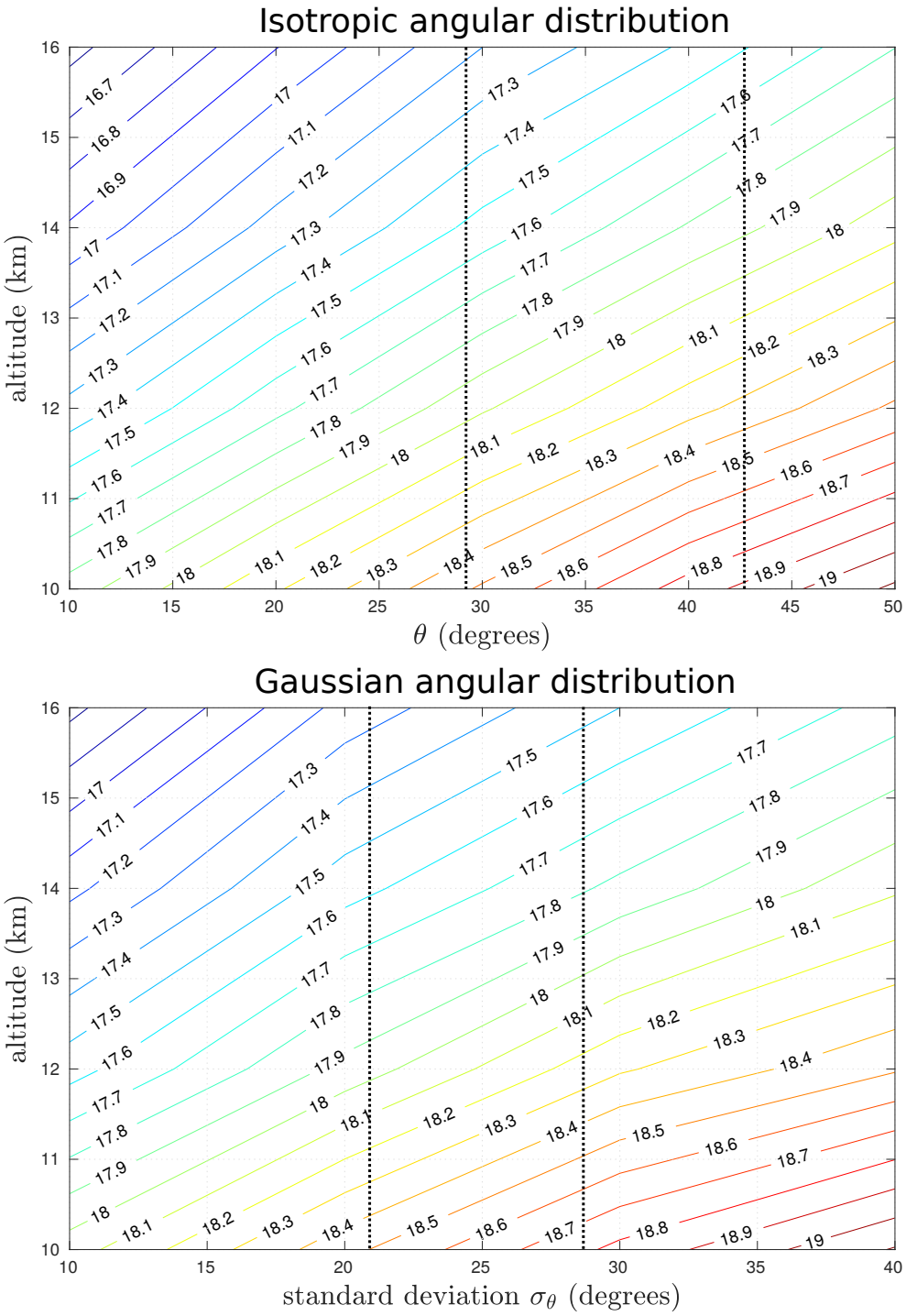

Figure 6. Level curves of the photon number intensity N_γ of the source TGF required for the simulation to produce the ≈160 counts recorded during the ASIM event 180916. It is expressed as function of altitude and opening angle, in decimal logarithm. The dotted lines demarcate the parameter space where the angular distribution has been constrained (see figure 4). **a.** Assuming that the source TGF has a isotropic angular distribution inside a cone, with half angle θ. **b.** Assuming a Gaussian angular distribution with standard deviation σ_θ.

6 Acknowledgments

This work was supported by the European Research Council under the European Union's Seventh Framework Program (FP7/2007-2013)/ERC grant agreement n. 320839 and the Research Council of Norway under contract 223252/F50 (CoE). ASIM is a mission of ESA's SciSpace Programme for scientific utilization of the ISS and non-ISS space exploration platforms and space environment analogues. This study has received funding from the European Union's Horizon 2020 research and innovation programme under the Marie Sklodowska-Curie grant agreement SAINT 722337. ASIM was funded through the ESA ELIPS program, through contracts with TERMA and Danish Technical University (DTU) in Denmark, University of Bergen (UB) in Norway and University of Valencia (UV) in Spain. Additional funding was supported by the ESA PRODEX contracts PEA 4000105639 and 4000111397 to DTU and ESA PRODEX contract 4000102100 and by Norwegian Research Council to UB. The ASIM Science Data Centre (ASDC) at DTU is supported by PRODEX contract PEA 4000115884 and by PRODEX contract PEA4000123438 at UB. The ASIM Science Data Centre and data analysis activities at the UV are supported by the MINECO Research Grants ESP2015- 69909-C5-1-R and ESP2017-86263-C4-1-R.

The GOES-R Advanced Baseline Imager data are available via the National Oceanic and Atmospheric Administration (NOAA) Comprehensive Large Array-data Stewardship System (CLASS).

The simulations were performed on resources provided by UNINETT Sigma2 - the National Infrastructure for High Performance Computing and Data Storage in Norway, under project no. NN9526K.

The Geant4-based model for Terrestrial Gamma-ray Flash (TGF) and associated electrons and positrons propagation in Earth atmosphere and environment (magnetic field) is available in the following GitHub repository: `https://github.com/DavidSarria89/TGF-Propagation-Geant4`, or the following DOI: `https://doi.org/10.5281/zenodo.2597039`.

The data described in this paper is available from the authors on request (david.sarria@uib.no) and a part of it can also be downloaded from the ASIM Science Data Centre (ASDC) homepage after a proposal has been submitted and approved.

Appendix A Geant4-based Monte-Carlo model of TGF and TEB propagation in the atmosphere, ionosphere and magnetosphere.

In order to estimate the response of MXGS-HED instrument for this event, we first needed to generate TGF (photons) and TEB (electrons and positrons) spectra just before they reach the International Space Station. We used a code based on the Geant4 toolkit (Agostinelli et al., 2003; Allison et al., 2006, 2016) to propagate particles in the atmosphere, ionosphere and magnetosphere. The code is available in an online repository, see acknowledgements. The geometry uses 256 exponentially spaced atmospheric layers between 1 and 150 km altitude (the atmosphere is negligible above) of constant density, composed only of N_2 and O_2, for simplicity and better performance. Densities within these layers are calculated with the NRLMSISE-00 model (Picone et al., 2002). The magnetic field of the Earth is modeled using the IGRF-12 model (Thébault et al., 2015). The propagation of photons, electrons and positrons is simulated, including all the relevant processes, which are included in the Geant4 toolkit. Different models can be used (semi-analytical, or database driven like Livermore, Penelope, among others), more-or-less accurate in the low energy part. In the context of photon/electron/positron propagation in air above 50 keV, and without electric fields, they all show similar results as long as the effects of straggling are included (Rutjes et al., 2016), that is the default behavior of Geant4.

The source TGF is assumed to be a point source with adjustable altitude, typically set between 10 and 16 km. The energy spectrum has an exponential distribution proportional to $1/\epsilon \exp\left(-\epsilon/\epsilon_{\mathrm{cut}}\right)$, with a cutoff $\epsilon_{cut} = 7.3$ MeV. The angular distribution is Gaussian with a standard deviation of 30 degrees, and has no tilt. The electrons, photons and positrons are collected at an altitude of 400 km, inside a circle of $R = 80$ km radius around the position of the ISS. The spectra can be built using this data, but to properly build the photon lightcurve, R should be less than 1 km (to avoid artificial time broadening). Figure A1 shows the recorded energy spectra at 400 km altitude. They were then used as an input to calculate the response of the ASIM mass model to the TGF and the TEB. The amplitude of the spectra shown in the figure are not representative of the fluences (particles/cm^2) of the different particle types. The real fluence ratio of positrons over electrons is about 0.13 (for other settings, it can fluctuate between 0.08 and 0.15). The real fluence ratio of electrons over photons is dependent on where the satellite is located with respect to the center of the TEB, on the offset between the TEB and the TGF

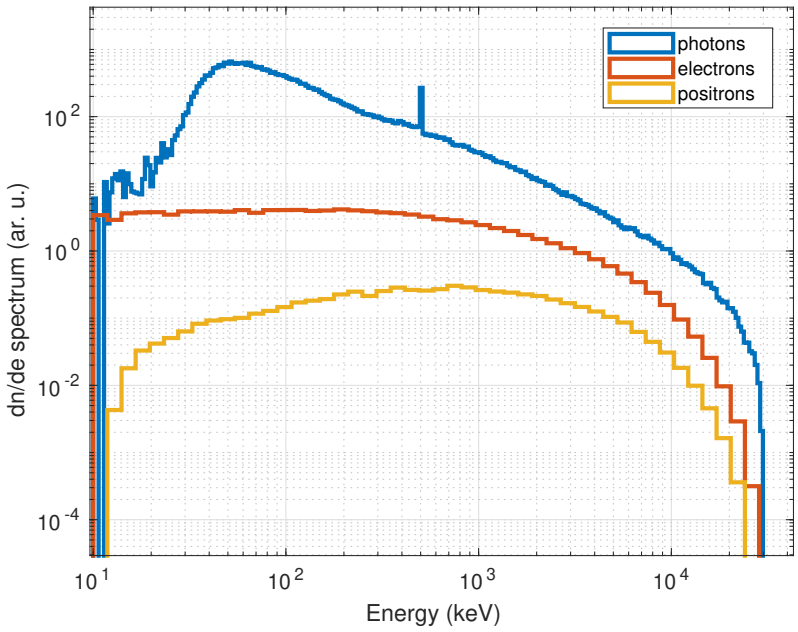

Figure A1. Results of the Geant4-based model simulation. Photon, electron and positron energy spectrum, recorded at 400 km altitude, within 80 km radial distance around the ISS position (i.e. in a plane perpendicular to the local vertical). The photon spectrum uses a finer binning to better represent the 511 keV line when this spectrum is used as input for the ASIM mass model. The initial source is a TGF at 15 km altitude and has a Gaussian angular distribution centered towards zenith with standard deviation of $\sigma_\theta = 30°$. The amplitude of the spectra shown here is not representative of the fluences (particles/cm^2) of the different particle types.

(which depends on the geographical location) and on the angular distribution of the TGF. Figure A2 presents the evolution of this ratio as function of the distance to the center of the electron beam and, an initial TGF with a Gaussian angular distribution with several values of σ_θ.

References

Agostinelli, S., Allison, J., Amako, K., Apostolakis, J., Araujo, H., Arce, P., ... others (2003, July). GEANT4 - a simulation toolkit. *Nuclear Instruments and Methods in Physics Research A, 506*, 250-303. doi: 10.1016/S0168-9002(03)01368-8

Allison, J., Amako, K., Apostolakis, J., Araujo, H., Dubois, P. A., Asai, M., ...

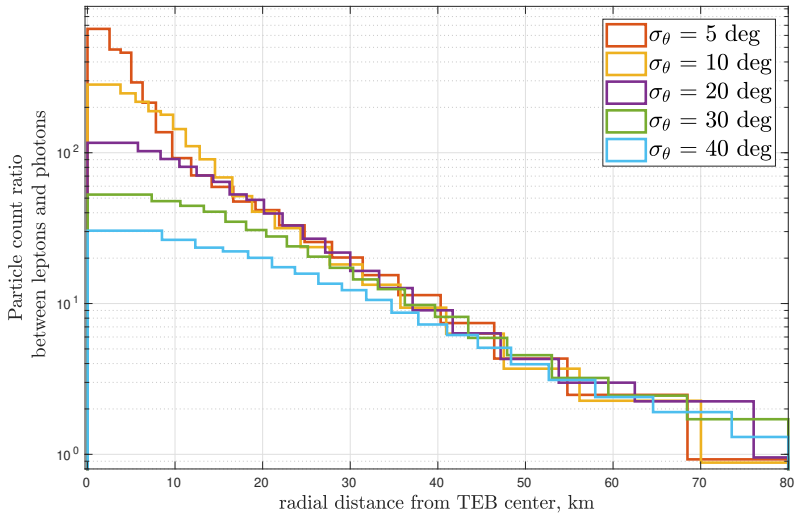

Figure A2. Simulated fluence ratio between photons (TGF) and leptons (TEB) for the ASIM 180916 event, where the ISS was located at about 650 km of the source TGF. The fluence ratio is presented as function of the distance between the ISS and the center of the electron beam, for several angular distributions (assuming a Gaussian distribution with parameter σ_θ). It also assumes that the source TGF is produced at 15 km altitude. The response of the MXGS detector (i.e. the relative detection efficiency between electrons and photons) is not taken into account here. Note that the real spatial distribution of the leptons is contained inside an ellipse and here the particles are recorded inside rings (circular symmetry) for simplicity.

others (2006, February). Geant4 developments and applications. *IEEE Transactions on Nuclear Science*, *53*, 270-278. doi: 10.1109/TNS.2006.869826

Allison, J., Amako, K., Apostolakis, J., Arce, P., Asai, M., Aso, T., ... Yoshida, H. (2016, November). Recent developments in GEANT4. *Nuclear Instruments and Methods in Physics Research A*, *835*, 186-225. doi: 10.1016/j.nima.2016.06.125

Briggs, M. S., Connaughton, V., Wilson-Hodge, C., Preece, R. D., Fishman, G. J., Kippen, R. M., ... Smith, D. M. (2011, January). Electron-positron beams from terrestrial lightning observed with Fermi GBM. Geophys. Res. Lett., *38*, L02808. doi: 10.1029/2010GL046259

Briggs, M. S., Fishman, G. J., Connaughton, V., Bhat, P. N., Paciesas, W. S., Preece, R. D., ... Chekhtman, A. (2010, July). First results on terrestrial gamma ray flashes from the Fermi Gamma-ray Burst Monitor. *Journal of Geophysical Research (Space Physics)*, *115*, A07323. doi: 10.1029/2009JA015242

Carlson, B. E., Gjesteland, T., & Østgaard, N. (2011, November). Terrestrial gamma-ray flash electron beam geometry, fluence, and detection frequency. *Journal of Geophysical Research (Space Physics)*, *116*, A11217. doi: 10.1029/2011JA016812

Chanrion, O., Neubert, T., Lundgaard Rasmussen, I., Stoltze, C., Tcherniak, D., Jessen, N. C., ... Lorenzen, M. (2019, June). The Modular Multispectral Imaging Array (MMIA) of the ASIM Payload on the International Space Station. Space Sci. Rev., *215*, 28. doi: 10.1007/s11214-019-0593-y

Cummer, S. A., Briggs, M. S., Dwyer, J. R., Xiong, S., Connaughton, V., Fishman, G. J., ... Solanki, R. (2014, December). The source altitude, electric current, and intrinsic brightness of terrestrial gamma ray flashes. Geophys. Res. Lett., *41*, 8586-8593. doi: 10.1002/2014GL062196

Dwyer, J. R., Grefenstette, B. W., & Smith, D. M. (2008, January). High-energy electron beams launched into space by thunderstorms. Geophys. Res. Lett., *35*, L02815. doi: 10.1029/2007GL032430

Dwyer, J. R., & Smith, D. M. (2005, November). A comparison between Monte Carlo simulations of runaway breakdown and terrestrial gamma-ray flash observations. Geophys. Res. Lett., *32*, L22804. doi: 10.1029/2005GL023848

Dwyer, J. R., Smith, D. M., & Cummer, S. A. (2012, November). High-Energy At-

mospheric Physics: Terrestrial Gamma-Ray Flashes and Related Phenomena. Space Sci. Rev., *173*, 133-196. doi: 10.1007/s11214-012-9894-0

Emmert, J. T., Richmond, A. D., & Drob, D. P. (2010, August). A computationally compact representation of Magnetic-Apex and Quasi-Dipole coordinates with smooth base vectors. *Journal of Geophysical Research (Space Physics)*, *115*, A08322. doi: 10.1029/2010JA015326

Gjesteland, T., Østgaard, N., Laviola, S., Miglietta, M. M., Arnone, E., Marisaldi, M., ... Montanya, J. (2015, December). Observation of intrinsically bright terrestrial gamma ray flashes from the Mediterranean basin. *Journal of Geophysical Research (Atmospheres)*, *120*, 12. doi: 10.1002/2015JD023704

Hazelton, B. J., Grefenstette, B. W., Smith, D. M., Dwyer, J. R., Shao, X.-M., Cummer, S. A., ... Holzworth, R. H. (2009, January). Spectral dependence of terrestrial gamma-ray flashes on source distance. Geophys. Res. Lett., *36*, L01108. doi: 10.1029/2008GL035906

Lefeuvre, F., Blanc, E., & Pinçon, J. L. (2009, April). TARANIS-a Satellite Project Dedicated to the Physics of TLEs and TGFs. In *American institute of physics conference series* (Vol. 1118, p. 3-7). doi: 10.1063/1.3137711

Mailyan, B. G., Briggs, M. S., Cramer, E. S., Fitzpatrick, G., Roberts, O. J., Stanbro, M., ... Dwyer, J. R. (2016, November). The spectroscopy of individual terrestrial gamma-ray flashes: Constraining the source properties. *Journal of Geophysical Research (Space Physics)*, *121*, 11. doi: 10.1002/2016JA022702

Marisaldi, M., Fuschino, F., Tavani, M., Dietrich, S., Price, C., Galli, M., ... Vercellone, S. (2014, February). Properties of terrestrial gamma ray flashes detected by AGILE MCAL below 30 MeV. *Journal of Geophysical Research (Space Physics)*, *119*, 1337-1355. doi: 10.1002/2013JA019301

Neubert, T., Østgaard, N., Reglero, V., Blanc, E., Chanrion, O., Oxborrow, C. A., ... Bhanderi, D. D. V. (2019, Mar 12). The asim mission on the international space station. *Space Science Reviews*, *215*(2), 26. Retrieved from `https://doi.org/10.1007/s11214-019-0592-z` doi: 10.1007/s11214-019-0592-z

Neubert, T., Østgaard, N., Reglero, V., Chanrion, O., Heumesser, M., K., D., ... J., E. C. (2019). A terrestrial gamma-ray flash and a transient luminous event powered by the same lightning discharge. *Science*. (Under review)

Østgaard, N., Balling, J. E., Bjørnsen, T., Brauer, P., Budtz-Jørgensen, C., Bu-

459 jwan, W., ... Yang, S. (2019, February). The Modular X- and Gamma-Ray
460 Sensor (MXGS) of the ASIM Payload on the International Space Station.
461 Space Sci. Rev., *215*, 23. doi: 10.1007/s11214-018-0573-7

462 Østgaard, N., Gjesteland, T., Stadsnes, J., Connell, P. H., & Carlson, B. (2008,
463 February). Production altitude and time delays of the terrestrial gamma
464 flashes: Revisiting the Burst and Transient Source Experiment spectra.
465 *Journal of Geophysical Research (Space Physics)*, *113*, A02307. doi:
466 10.1029/2007JA012618

467 Østgaard, N., Neubert, T., Reglero, V., K., U., S., Y., G., G., ... S., A.-N. (2019).
468 First ten months of TGF observations by ASIM. *Journal of Geophysical Re-*
469 *search (Atmospheres)*. (Submitted)

470 Picone, J. M., Hedin, A. E., Drob, D. P., & Aikin, A. C. (2002, December).
471 NRLMSISE-00 empirical model of the atmosphere: Statistical comparisons
472 and scientific issues. *Journal of Geophysical Research (Space Physics)*, *107*,
473 1468. doi: 10.1029/2002JA009430

474 Roberts, O. J., Fitzpatrick, G., Stanbro, M., McBreen, S., Briggs, M. S., Holzworth,
475 R. H., ... Mailyan, B. G. (2018, May). The First Fermi-GBM Terrestrial
476 Gamma Ray Flash Catalog. *Journal of Geophysical Research (Space Physics)*,
477 *123*, 4381-4401. doi: 10.1029/2017JA024837

478 Rutjes, C., Sarria, D., Broberg Skeltved, A., Luque, A., Diniz, G., Østgaard, N., &
479 Ebert, U. (2016, November). Evaluation of Monte Carlo tools for high energy
480 atmospheric physics. *Geoscientific Model Development*, *9*, 3961-3974. doi:
481 10.5194/gmd-9-3961-2016

482 Sarria, D., Blelly, P.-L., Briggs, M. S., & Forme, F. (2016, May). Studying the time
483 histogram of a terrestrial electron beam detected from the opposite hemisphere
484 of its associated TGF. *Journal of Geophysical Research (Space Physics)*, *121*,
485 4698-4704. doi: 10.1002/2015JA021881

486 Sarria, D., Blelly, P.-L., & Forme, F. (2015, May). MC-PEPTITA: A Monte Carlo
487 model for Photon, Electron and Positron Tracking In Terrestrial Atmosphere.
488 Application for a terrestrial gamma ray flash. *Journal of Geophysical Research*
489 *(Space Physics)*, *120*, 3970-3986. doi: 10.1002/2014JA020695

490 Sarria, D., Lebrun, F., Blelly, P.-L., Chipaux, R., Laurent, P., Sauvaud, J.-A., ...
491 Lindsey-Clark, M. (2017, July). TARANIS XGRE and IDEE detection

capability of terrestrial gamma-ray flashes and associated electron beams. *Geoscientific Instrumentation, Methods and Data Systems*, *6*, 239-256. doi: 10.5194/gi-6-239-2017

Smith, D. M., Lopez, L. I., Lin, R. P., & Barrington-Leigh, C. P. (2005, February). Terrestrial Gamma-Ray Flashes Observed up to 20 MeV. *Science*, *307*, 1085-1088. doi: 10.1126/science.1107466

Thébault, E., Finlay, C. C., Beggan, C. D., Alken, P., Aubert, J., Barrois, O., ... Zvereva, T. (2015, May). International Geomagnetic Reference Field: the 12th generation. *Earth, Planets, and Space*, *67*, 79. doi: 10.1186/s40623-015-0228-9

Ursi, A., Guidorzi, C., Marisaldi, M., Sarria, D., & Frontera, F. (2017, April). Terrestrial gamma-ray flashes in the BeppoSAX data archive. *Journal of Atmospheric and Solar-Terrestrial Physics*, *156*, 50-56. doi: 10.1016/j.jastp.2017.02.014